Resolution of the system of the ideal magnetohydrodynamics by a finite-volume kinetic-type method

R. Khanfir [a], G. Chanteur [b], J.P. Croisille [c]

[a] *Département de Mathématiques, Université d'Evry-Val-d'Essonne, Boulevard des Coquibus, 91025 Evry, France, e-mail: khanfir@lami.univ-evry.fr*

[b] *Centre d'Etude des Environnements Terrestres et Planétaires, 10-12 avenue de l'Europe, 78140 Vélizy, France, e-mail: gerard.chanteur@cetp.ipsl.fr*

[c] *Laboratoire d'Analyse Numérique d'Orsay, Bât.425, Université Paris Sud, 91405, Orsay Cedex, France, e-mail: Jean-Pierre.CROISILLE@math.u-psud.fr*

The numerical investigation of a finite volume scheme for the ideal MHD, introduced by the authors in a preceding paper, is pursued. This scheme is based on an original flux-splitting formula, partly kinetic based. It is simple, robust and is inherently consistent with the equation $\nabla . B = 0$ on the magnetic field. Numerical tests in one and two dimensions with the second order version of the scheme are displayed, showing its efficiency. The numerical dissipation is estimated.

1 Introduction

The aim of this paper is to present an efficient second order finite volume scheme for the hyperbolic system of ideal MHD. The numerical simulation of these equations receives today a renewed interest among applied mathematicians and computer physicists. The former try to extend the ideas successfully designed for the Euler equations, to the non strictly hyperbolic and non convex MHD system . The latter need efficient methods able to compute accurate solutions on unstructured and adaptive grids required to tackle large scale problems involving sharply localized transition regions in space plasmas. Many schemes have been recently developed for the MHD equations. Stone and Norman [23,24] designed a finite difference method in orthogonal curvilinear coordinates for astrophysical flows. Zalesak et al [28] emphasized the importance of adaptative mesh refinement allowed by finite element methods, subsequently de Fainchtein et al [11] demonstrated the ability of this method to simulate MHD turbulence. Tanaka [25] elaborated a finite volume scheme of

Preprint submitted to Elsevier Preprint *12 April 1996*

TVD type (total variation diminishing) for the MHD modelling of planetary magnetospheres. A lot of work has been devoted to approximate Riemann solvers by Brio and Wu [4], Collela and Zachary [6] and Dai and Woodward [8]. All these schemes are explicit in time and resolve the fastest time scale imposed by the fast mode. Implicit or semi-implicit methods, for example Lerbinger and Luciani [17], are required to investigate dissipative processes which generally occur on much longer time scales.

This article proposes a generalization to the ideal MHD of kinetic solvers [18–21] having the property to give upwind numerical fluxes. We emphasize the consistency of our MHD numerical flux with the $\nabla.B = 0$ equation. The outline of the paper is as follows. We recall in section 2 the flux-splitting formula introduced in [7]. Then the implementation of second order accuracy by MUSCL interpolation is presented (monotonic upstream scheme for conservation laws). Sections 4 and 5 are devoted to numerous 1d and 2d test case problems and section 6 gives conclusions and perspectives.

2 A finite volume scheme for the MHD

2.1 *Numerical flux*

The equations of ideal MHD (1) describe respectively the conservation of mass, momentum, total energy and magnetic flux (or Faraday's equation), the magnetic permeability of the vacuum μ_0 being taken into account by the substitution of $\dfrac{B}{\sqrt{\mu_0}}$ by B:

$$\left\{\begin{aligned} \frac{\partial \rho}{\partial t} + \nabla.(\rho u) &= 0, \\ \frac{\partial (\rho u)}{\partial t} + \nabla.(\rho u \otimes u + (p + \frac{|B|^2}{2})I - B \otimes B) &= 0, \\ \frac{\partial \rho\overline{e}}{\partial t} + \nabla.\left((\rho\overline{e} + p + \frac{|B|^2}{2})u - u.BB\right) &= 0, \\ \frac{\partial B}{\partial t} + \nabla.(B \otimes u - u \otimes B) &= 0, \\ \nabla.B &= 0, \end{aligned}\right. \tag{1}$$

where $\rho\overline{e} = \rho\varepsilon + \rho|u|^2/2 + |B|^2/2$ is the total energy, $\rho\varepsilon = p/(\gamma - 1)$ is the internal energy with γ the adiabatic index of the plasma. Introducing the conservative state vector $w = (\rho, \rho u, \rho\overline{e}, B)^t$ and its flux $F(w)$ allows to rewrite

(1) as:

$$\partial_t w + \nabla.F(w) = 0 \qquad \nabla.B = 0.$$

Let us briefly recall the first order finite volume scheme introduced in [7] on an unstructured grid (e.g. a triangular grid). The area of cell K is $|K|$ and the length of edge e is $|e|$. Assuming a constant state vector over each cell the basic scheme reads:

$$w_K^{n+1} = w_K^n - \frac{\Delta t}{|K|} \sum_{e \in \partial K} |e| F_{num}(w_K^n, w_{K_e}^n, n_e), \tag{2}$$

w_K^n is the state vector in cell K at time $n\Delta t$, $w_{K_e}^n$ is the state vector in the external cell adjacent to cell K on edge e, Δt is the time-step, F_{num} is the numerical flux through the edge e, n_e is the external normal to e.
The numerical flux F_{num} has to meet three requests:

(i) consistency with the physical flux F for each w and each vector n_e, i.e. $F_{num}(w, w, n_e) = F(w).n_e$.
(ii) conservativity, i.e. for each w_1, w_2, n_e, $F_{num}(w_1, w_2, n_e) = -F_{num}(w_2, w_1, n_e)$.
(iii) numerical stability under a not too restrictive CFL condition.

The numerical flux reads in flux-splitting form

$$F_{num}(w_1, w_2, n_e) = F_{num}^+(w_1, n_e) + F_{num}^-(w_2, n_e),$$

$F_{num}^+(w_1, n_e)$ represents the part of the flux crossing the edge e in the sense of n_e. This flux depends only on the state w_1 and the vector n_e. Similarly $F_{num}^-(w_2, n_e)$ represents the part of the flux crossing e in the direction of $-n_e$. Croisille et al [7], derived $F_{num}^+(w, n)$ in the following form

$$F_{num}^+(w, n) = \mathcal{F}^+(w, n).n$$

where $\mathcal{F}^+(w, n)$ is the tensor:

$$\mathcal{F}^+(w, n) = w \otimes u^+ + \left(0, P^+, \frac{1}{2}u.P^+ + \frac{1}{2}u^+.P, -u^+ \otimes B, \right)^t \tag{3}$$

$u^+(w, n)$ and $P^+(w, n)$ play the role of an "upwind" speed and an "upwind" pressure tensor along the direction of n.

$$\begin{aligned} u^+(w, n) &= \alpha\left(-\tfrac{u.n}{T}\right) u + C\,\beta\left(-\tfrac{u.n}{T}\right) n \\ P^+(w, n) &= \alpha\left(-\tfrac{u.n}{T}\right) P \end{aligned}$$

where P is the MHD tensor $P = \overline{p}\,I - B \otimes B$, T is an equivalent temperature given by $T = \overline{p}/\rho$, with $\overline{p} = p + |B|^2/2$ the total pressure, C is an equivalent "thermal" speed $C = (2T)^{1/2}$, α and β are the special functions

$$\alpha(z) = \frac{1}{2} erfc(z); \; \beta(z) = \frac{1}{2\pi^{1/2}} exp(-z^2).$$

We refer to [7] for a justification of formula (3) by kinetic arguments. Notice that scheme (2) is of first order in space and time.

2.2 Consistency with $\nabla.B = 0$

In this section, we prove an important feature of scheme (2), namely its consistency with the $\nabla.B = 0$ equation on any conformal triangulation of finite-element type. Recall that this equation is in "involution" with the four conservation laws of the MHD, what means that $\nabla.B = 0$ at the initial time implies $\nabla.B(t) = 0$ for $t > 0$. This consistency property is difficult to obtain with finite volume schemes based on Approximate Riemann Solvers. In some of them, $\nabla.B = 0$ has to be forced as a constraint at each time step, whereas in others, it is simply forgotten. In our case, the consistency results from a general interesting property pointed out by F. Bouchut [3]. Suppose

$$B_K^{n+1} = B_K^n - \frac{\Delta t}{|K|} \sum_{e \in \partial K} |e| F_e(B_K^n, B_{K_e}^n, n_e) \qquad (4)$$

is a conservative finite volume scheme where the numerical flux $F_e(B_K^n, B_{K_e}^n, n_e)$ is orthogonal to the normal n_e (i.e. parallel to the face e). Let φ_S be any piecewise affine function of "hat" type, that is, belonging to the standard basis of the P^1-Lagrange finite element space attached to the triangulation. Then $\langle \nabla.(B^{n+1} - B^n), \varphi_S \rangle = 0$ where $\langle , \rangle$ is the duality bracket $\langle \nabla.B, \varphi_S \rangle = -(B, \nabla\varphi_S)_{L^2}$ (distribution sense). So, $\langle \nabla.B^0, \varphi_S \rangle = 0$ implies $\langle \nabla.B^n, \varphi_S \rangle = 0$, which is clearly a consistency property of the scheme with the equation $\nabla.B = 0$. The proof is as follows. Denoting by $\mathcal{S}$ the support of φ_S ($\mathcal{S}$ is the union of the cells K having S as vertex,see Fig. 1), one has

$$\langle \nabla.(B^{n+1} - B^n), \varphi_S \rangle = \Delta t \sum_{K \in \mathcal{S}} \sum_{e \in \partial K} |e| \nabla\varphi_S . F_e(B_K^n, B_{K_e}^n, n_e) \qquad (5)$$

On K, the gradient of φ_S is constant and its value is given by $\nabla\varphi_S = -|e_{K,S}| n_{K,S}/2|K|$. Thus $\nabla\varphi_S . F_{e_{K,S}}(B_K^n, B_{K_e}^n, n_e) = 0$ since by hypothesis $F_{e_{K,S}} . n_{K,S} = 0$. So, the summation on $e \in \partial K$ in (5) has to be taken only onto $e \in \partial K \setminus \partial\mathcal{S}$. Inverting the two summation symbols in (5), taking

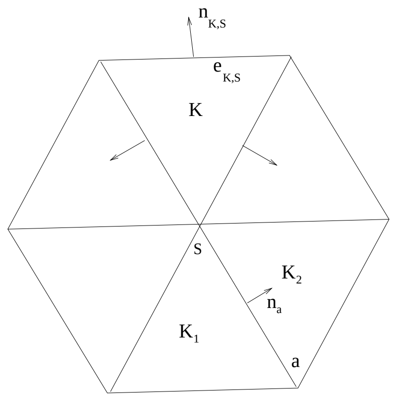

Fig. 1. Support of φ_S, a piecewise affine function taken in the standard basis of P^1-Lagrange finite element space attached to the triangulation.

into account that $F_e(B^n_K, B^n_{K_e}, n_e) = -F_e(B^n_{K_e}, B^n_K, -n_e)$ and denoting by $\mathcal{A}$ the set of the oriented edges from cell 1 to cell 2, (5) can be rewritten as

$$\langle \nabla.(B^{n+1} - B^n), \varphi_S \rangle = \Delta t \sum_{a \in \mathcal{A}} |a| (\nabla \varphi_{K_2} - \nabla \varphi_{K_1}).F_a(B^n_{K_1}, B^n_{K_2}, n_a) \quad (6)$$

Since $\varphi_{K_1} = \varphi_{K_2}$ onto a and since F_a is by hypothesis in the vector space $n_a^\perp$ for each $a \in \mathcal{A}$ one has $\nabla \varphi_{K_1}.F_a = \nabla \varphi_{K_2}.F_a$, so each term of the sum (6) is zero, which implies that $\langle \nabla.(B^{n+1} - B^n), \varphi_S \rangle = 0$.

Note that this property is also true in three dimensions onto a tetrahedral mesh.

3 Second order extension of the bidimensional scheme

3.1 The second order spatial scheme

A higher order scheme in space is obtained by replacing in (2) the term $F_{num}(w_K, w_{K_e}, n_e)$ by $F_{num}(\tilde{w}_K, \tilde{w}_{K_e}, n_e)$, where $\tilde{w}_K$ is the value onto e of an affine interpolation of w on K. This interpolation is obtained by some extension to the unstructured context of the well-known "MUSCL" method introduced by Van-Leer [27].
There are two steps:

(i) Interpolation step:
Let θ be the constant value of any scalar variable of the system on the cell K; θ_j are the values of the same variable on the adjacent cells K_j.

We compute by least-square the gradient of θ on cell K by minimizing

$$F(X,Y) = \frac{1}{2}\sum_{k=1}^{3}(\theta + X(x_k - x_0) + Y(y_k - y_0) - \theta_k)^2, \tag{7}$$

$\nabla\theta_K = X\,i + Y\,j$ is the unknown, $G(x_0, y_0)$, $G_k(x_k, y_k)$ are the barycenters of K, K_k. The linear interpolation on cell K is defined, for $M \in K$ by

$$\theta_K(M) = \theta + \nabla\theta_K.GM.$$

The solution is given by

$$X = (c_1 b_2 - c_2 b_1)/\Delta, \qquad Y = (a_1 c_2 - a_2 c_1)/\Delta$$

where

$$a_1 = \sum_k (x_k - x_0)^2, \;\; a_2 = b_1 = \sum_k (x_k - x_0)(y_k - y_0), \;\; b_2 = \sum_k (y_k - y_0)^2$$

$$c_1 = \sum_k (x_k - x_0)(\theta_k - \theta),\; c_2 = \sum_k (y_k - y_0)(\theta_k - \theta),\; \Delta = a_1 b_2 - a_2 b_1.$$

In this way a first order approximation of the gradient of θ is obtained.

(ii) Limitation step:
The implementation of this reconstruction method without flux limiters is known to produce spurious oscillations. In order to avoid this artefact we apply a local monotonicity criterion [13]. Let θ_k be the value of the reconstructed solution at the intersection point M_k between the k-th edge of cell K and the $[G, G_k]$ segment (Fig. 2). We define

$$\begin{cases} \Delta\theta_k = \dfrac{|GM_k|}{|GG_k|}(\theta_k - \theta), \\ \Delta_k \;\; = \nabla\theta.GM_k, \end{cases} \tag{8}$$

The limited value of the gradient is

$$(\nabla\theta)_L = \begin{cases} \nabla\theta\,\varphi\left(\frac{\Delta\theta_1}{\Delta_1}\right)\,\varphi\left(\frac{\Delta\theta_2}{\Delta_2}\right)\,\varphi\left(\frac{\Delta\theta_3}{\Delta_3}\right), & \text{for } \Delta_1.\Delta_2.\Delta_3 \neq 0, \\ 0, & \text{for } \Delta_1.\Delta_2.\Delta_3 = 0. \end{cases} \tag{9}$$

where φ is some limitation function, e.g. the min-mod function given by

$$\varphi(r) = \begin{cases} 0, & \text{for } r < 0, \\ r, & \text{for } 0 < r < 1, \\ 1, & \text{for } r > 1. \end{cases}$$

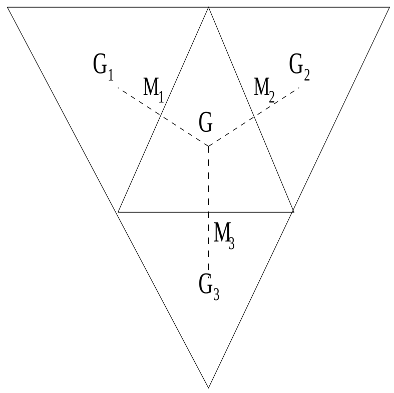

Fig. 2. Interface points chosen to compute the solution on the edges in the second order version of the scheme.

Other extension methods to "second order" accuracy on unstructered meshes have been proposed [2,9,26]. We give in section 4.4 a numerical estimation of the effective order of the scheme in 1d.

3.2 Summary of the second order algorithm

A second order Runge-Kutta scheme is used for the discretization in time. So the final algorithm consists of a prediction step on a half time-step $\Delta t/2$ with the first order spatial discretization, followed by a correction step on Δt using the reconstructed piecewise linear solution.

We give now the final form of the second order algorithm. The unknown w_K^{n+1} are computed from the known values w_K^n in three steps summarized as follows:

prediction step

$$\tilde{w}_K = w_K^n - \frac{\Delta t}{2|K|} \sum_{e \in \partial K} |e| \left(\mathcal{F}^+(w_K^n, n_e) + \mathcal{F}^-(w_{K_e}^n, n_e) \right) .n_e$$

reconstruction step If $\tilde{V}_K = (\tilde{\rho}_K, \tilde{u}_K, \tilde{p}_K, \tilde{B}_K)$ is the non conservative state vector corresponding to $\tilde{w}_K$, the k-interface values, $\tilde{V}_e^{\pm}$, are reconstructed by

$$\tilde{V}_e^- = \tilde{V}_K + \left(\nabla \tilde{V}_K \right)_L .GM_k$$
$$\tilde{V}_e^+ = \tilde{V}_{K_e} + \left(\nabla \tilde{V}_{K_e} \right)_L .G_k M_k$$

correction step

$$w_K^{n+1} = w_K^n - \frac{\Delta t}{|K|} \sum_{e \in \partial K} |e| \left(\mathcal{F}^+(\tilde{w}_e^-, n_e) + \mathcal{F}^-(\tilde{w}_e^+, n_e) \right) .n_e$$

where $\tilde{w}_e^{\pm}$ is the conservative variable corresponding to $\tilde{V}_e^{\pm}$

4 One-dimensional numerical tests

We present three one-dimensional tests cases of MHD simple waves computed with the second order scheme: two coplanar Riemann problems ($B_z = u_z = 0$) and a non linear Alfvén wave. Other validation tests are given in [14] for linearized MHD waves.

4.1 Brio and Wu's test case

This coplanar Riemann problem [4] consists of two constant initial states: $(\rho_l = 1, u_l = 0, B_l = (0.75, 1, 0), p_l = 1)$; $(\rho_r = 0.125, u_r = 0, B_r = (0.75, -1, 0)$, $p_r = 0.1)$. The adiabatic index is $\gamma = 2$, we use a mesh of 800 cells of length $\Delta x = 1$ with a Courant number equal to 0.4.
The solution at time $T = 80$ is displayed on Fig. 3 and we identify the following waves: a fast rarefaction propagating to the left, a compound wave propagating to the left made of an intermediate shock (B_y changes its sign) and a slow rarefaction attached to it, a contact discontinuity, a slow shock propagating to the right, a fast rarefaction propagating to the right. The existence of the compound wave is due to the non-convexity of the MHD system; when B_y crosses the zero-value, the eigenvector associated to the slow eigenmode changes its nature from genuinely non linear to linearly degenerated. The results obtained by our solver are in very good agreement with those obtained by other solvers [4,6,8].

4.2 Colella and Zachary's test case

This Riemann problem [6] is a transverse MHD flow ($B_x = 0$) [15] and its solution may be computed analytically as in the Euler case. The left and right states are given by: $(\rho_l = 1, u_l = 0, B_l = (0., 1, 0), p_l = 1000)$; $(\rho_r = 0.125, u_r = 0, B_r = (0, -1, 0), p_r = 0.1)$. There is a jump of 10^4 in the thermal pressure across the discontinuity. The adiabatic index is $\gamma = 2$, we use a mesh of 400 cells of length $\Delta x = 1$ with a Courant number equal to 0.8. The exact solution and the computed one are plotted on Fig. 4 which shows a very good superposition except around the contact discontinuity. The magnetic field evolves like the density ρ because $\dfrac{B_y}{\rho}$ is solution of the following pure transport equation,

$$\partial_t \left(\frac{B_y}{\rho} \right) + u_x \partial_x \left(\frac{B_y}{\rho} \right) = 0, \tag{10}$$

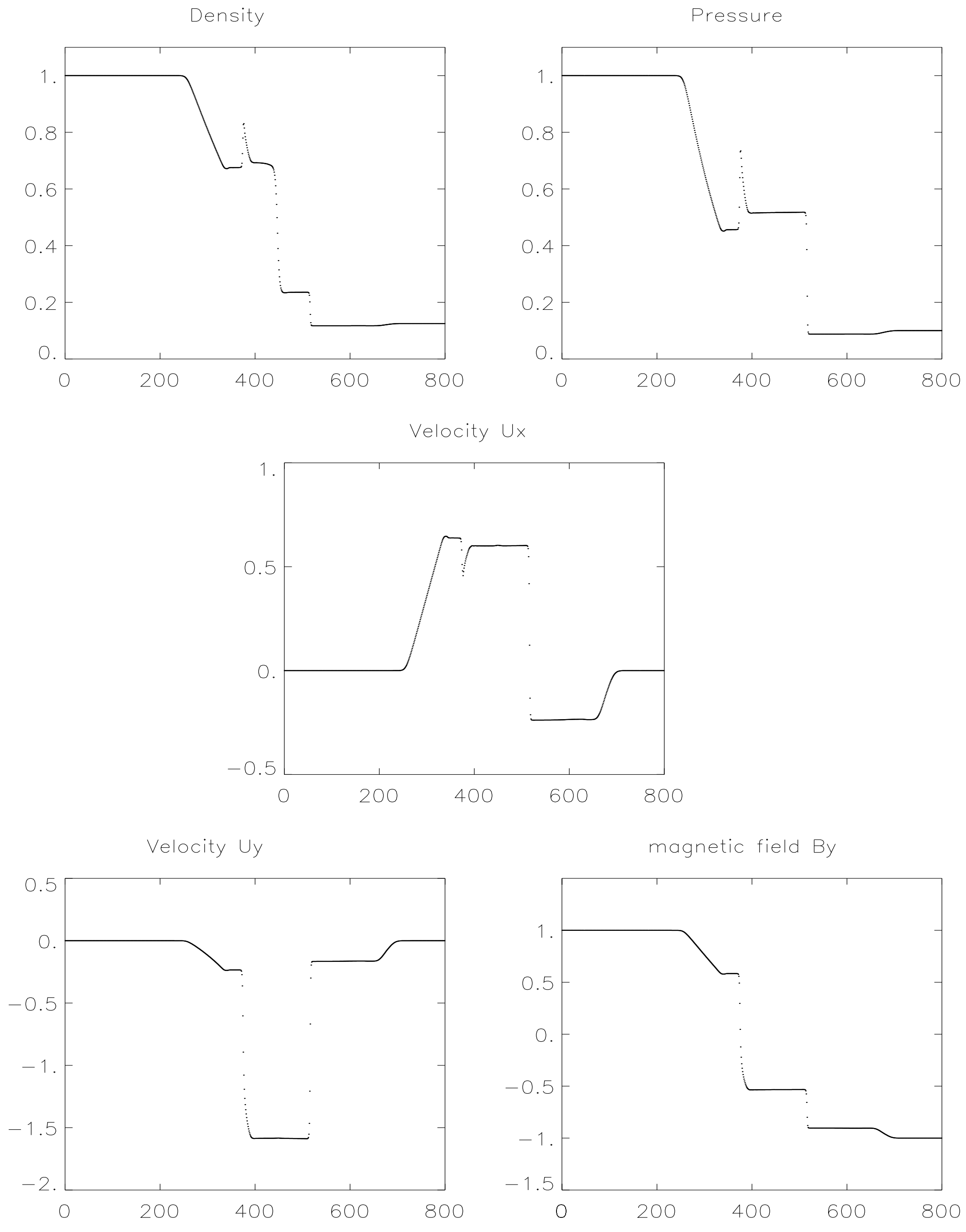

Fig. 3. Brio & Wu's test case at time $T = 80$. The peak values of the compound wave are for $\rho : 0.83, p : 0.74, u_x : 0.47$, the Courant number is 0.4.

The system can be reduced to a pure Euler one with the fast mode velocity $c_r = \sqrt{a^2 + B_y^2/\rho}$, instead of the sound speed a.

4.3 Nonlinear Alfvén wave

The initial condition corresponding to this time-independant simple wave is

$$\rho = 1, B_x = u_x = 0, u_t(x,t) = \frac{B_t(x,t)}{\sqrt{\rho}}, \text{ and } p^* = p + |B_t|^2/2 = 1.5.$$

The adiabatic index γ is equal to 5/3. The transverse components u_t and B_t, i.e. orthogonal to the x-direction, just rotate, thus $B_y = B_0 \sin\theta$, $B_z = B_0 \cos\theta$, $\theta(x)$ may be arbitrary; for this case we chose

$$\theta(x) = \pi(1 - \tanh(\frac{x - x_0}{l})),\ x_0 = 150,\ l = 80.$$

There are 800 cells of lenght $\Delta x = 1$ and the Courant number is equal to 0.4. The exact solution and the numerical one after 1900 time-steps ($T = 465$) are displayed on Figure 5 and are exactly superposed.

4.4 Effective order of the scheme

One can estimate the effective order of the scheme by computing the error between the exact and numerical solutions on different grids for test case (4.3) where cells have length Δx. More precisely, following Durlofsky et al [10] we define the $L^p(\Omega)$-error ($p = 1, 2$) at a fixed time T by

$$E_p(T) = \frac{|U(T) - U_{exact}(T)|_{L^p(\Omega)}}{|U_{exact}(T)|_{L^p(\Omega)}}.$$

This error is written in the form

$$E_p(T) = c\,\Delta x^\alpha,$$

and α is the effective order of the scheme. Tables 1 and 2 show the different values of the order for various quantities in the L^1 and the L^2 norms of the error. We used grids of respectively 100, 200, 400 and 800 cells.

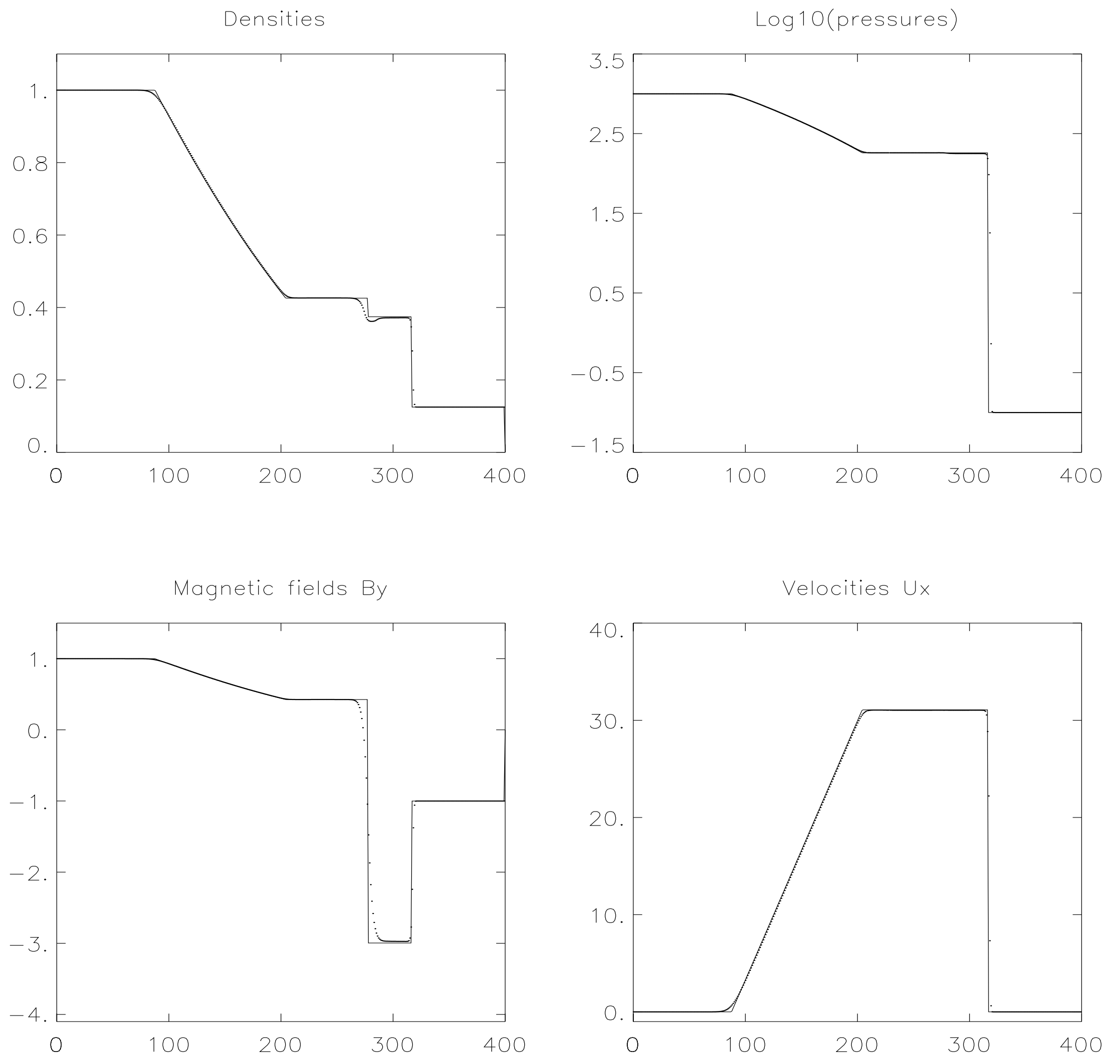

Fig. 4. Colella & Zachary's test case ($Bx = 0.00$) after 200 timesteps. Superposition of the exact (——) and computed solutions.

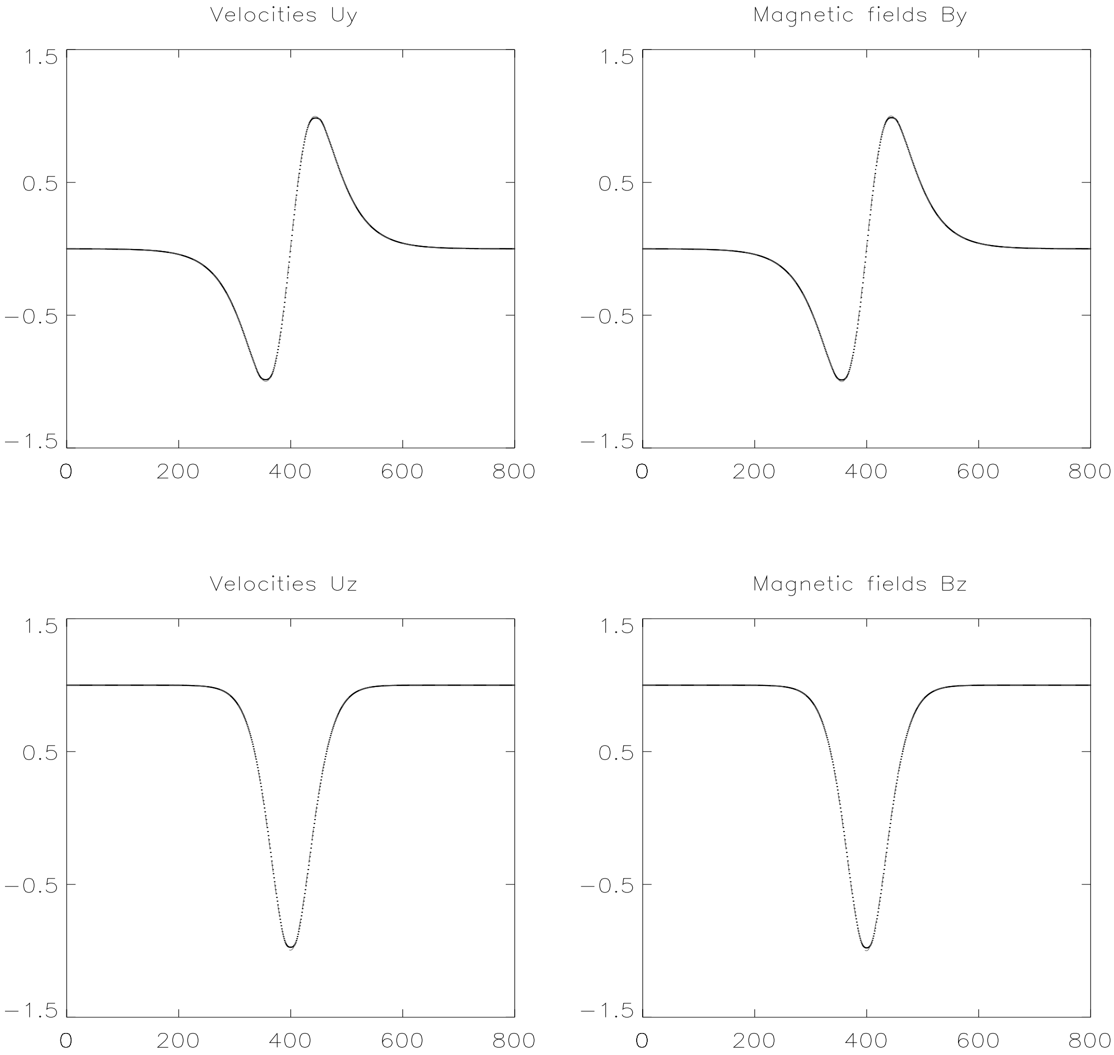

Fig. 5. Non linear Alfvén wave: $B_x = u_x = 0$, solution after ≈ 1900 timesteps. The B_t and u_t profiles are very well conserved.

quantity	L^1-norm	L^2-norm
ρu_y	0.608	0.548
B_y	0.608	0.548
ρu_z	0.614	0.569
B_z	0.614	0.569

Table 1: Numerical effective order with the first order version of the scheme

quantity	L^1-norm	L^2-norm
ρu_y	1.744	1.584
B_y	1.788	1.610
ρu_z	1.741	1.513
B_z	1.772	1.552

Table 2: Numerical effective order with the second order version of the scheme

5 Two-dimensional tests

We present two test-cases which are particular solutions of the MHD system. Although the exact solutions are of axisymmetric type, the numerical solutions are computed for the true 2d equations in cartesian coordinates. The computing domain is a disk of radius $R_0 = 1$ and we use two homogeneous Delaunay triangulations of 8000 and 32000 cells. The Courant number is equal to 0.4.

5.1 Alfvenic Vortex

We test the scheme with the following time-independant, incompressible flow:

$$\rho = \rho_0,\ u(r,t) = \frac{B(r,t)}{\sqrt{\rho_0}},\ B = (B_r = 0, B_\theta, B_z)\,,\ p = P_0 - |B|^2/2,$$

where the suffixes r, θ, z indicate respectively the radial, azimuthal and axial components of the fields; ρ_0 and P_0 are constants and B_θ and B_z may have any profiles. We show [14] that the previous state is a particular solution of the MHD system. We choose Bessel profiles in order to estimate the numerical diffusion coefficients of the scheme, as will be shown later. Thus we take

$$\begin{cases} B_\theta(r,t) = B_\theta^0 J_1(\alpha \frac{r}{R_0}), \\ B_z(r,t) = B_z^0 J_0(\beta \frac{r}{R_0}), \end{cases}$$

where J_0 and J_1 are respectively the zeroth and first order Bessel functions and α and β their first zeroes. The adiabatic index is taken to be 5/3. The boundary conditions are $B.n = u.n = 0$, which is a sufficient condition to ensure the stability of the solution (Chandrasekhar [5]).
Figures 6 and 7 display the exact solution (identical to the initial state), the first and second order computed solutions on the 8000-cells mesh after 1000 time-iterations. These figures are obtained by a least-square interpolation of the clouds of points representing the projection of the different values on the radius, by polynomials of degree three. Fig. 6 (resp. Fig. 7) represents the azimuthal (resp. axial) components of the velocity and the magnetic field. We can see that the numerical diffusion affects differently these two components: there is more diffusion on the velocity. The axisymmetry is well conserved.

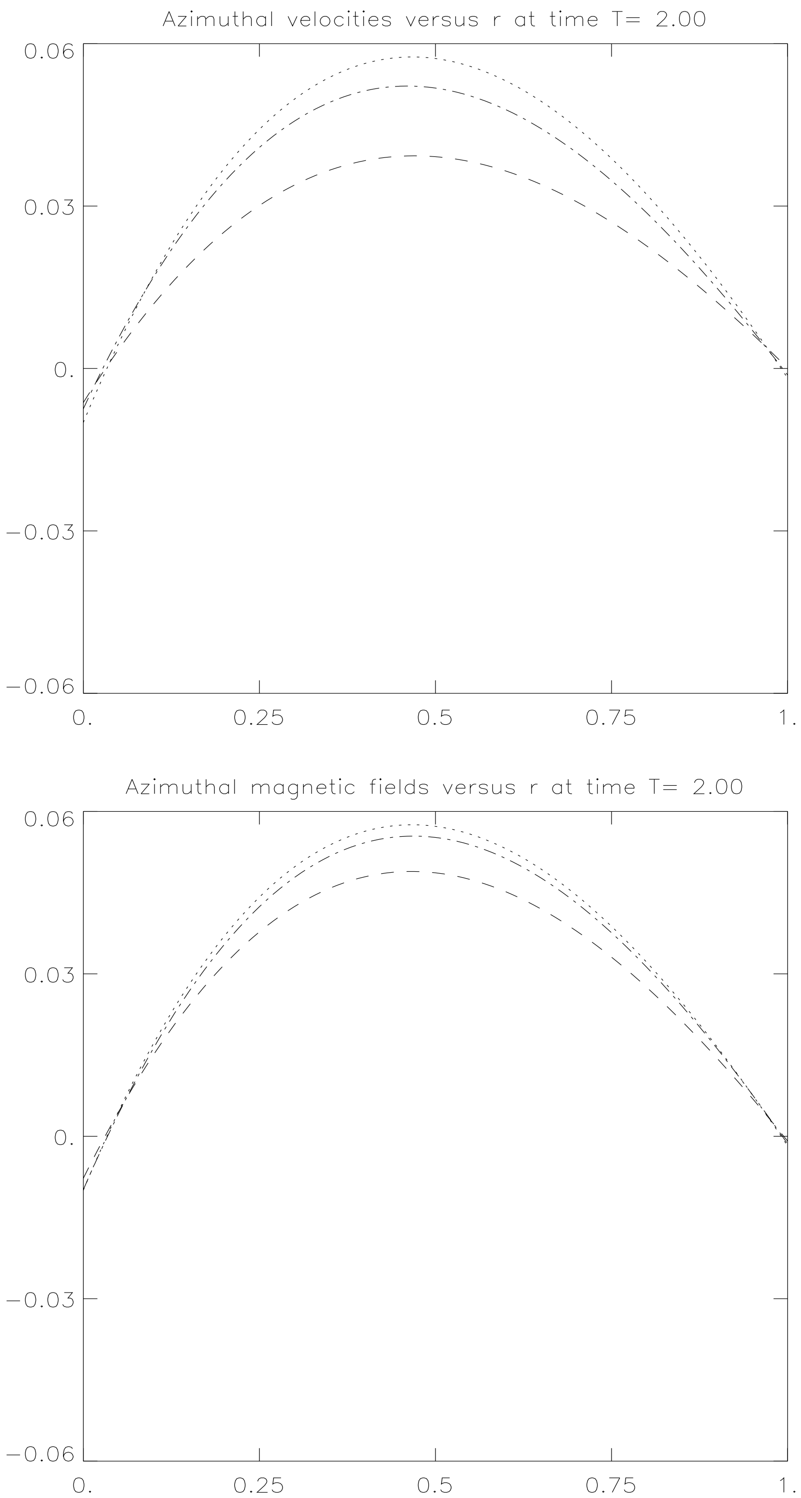

Fig. 6. Azimuthal components after 1000 time-iterations of the velocities and magnetic fields: superposition of exact $(\cdots\cdots)$, first order $(- - -\,-)$ and second order $(- \cdot - \cdot -)$ solutions.

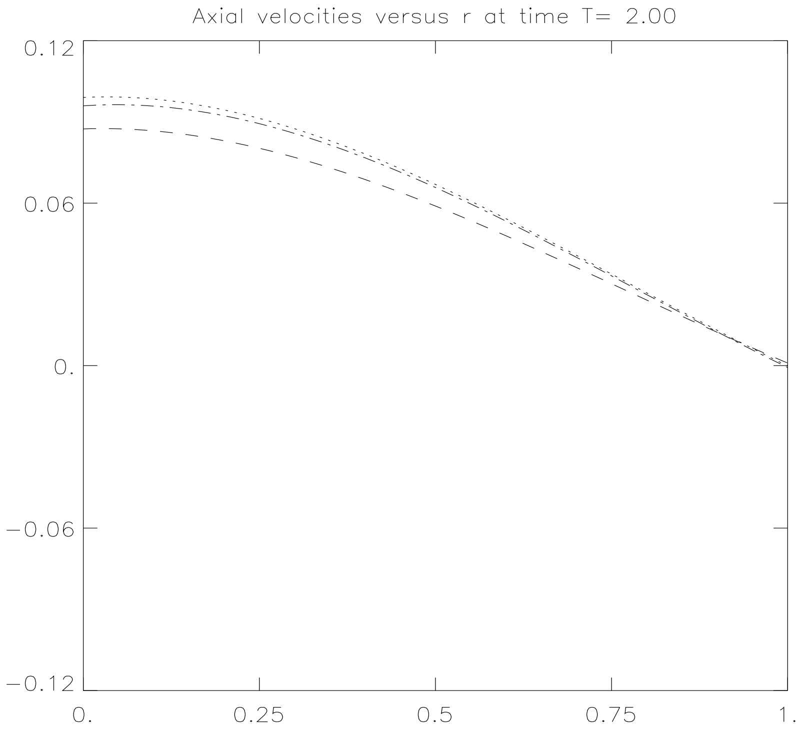

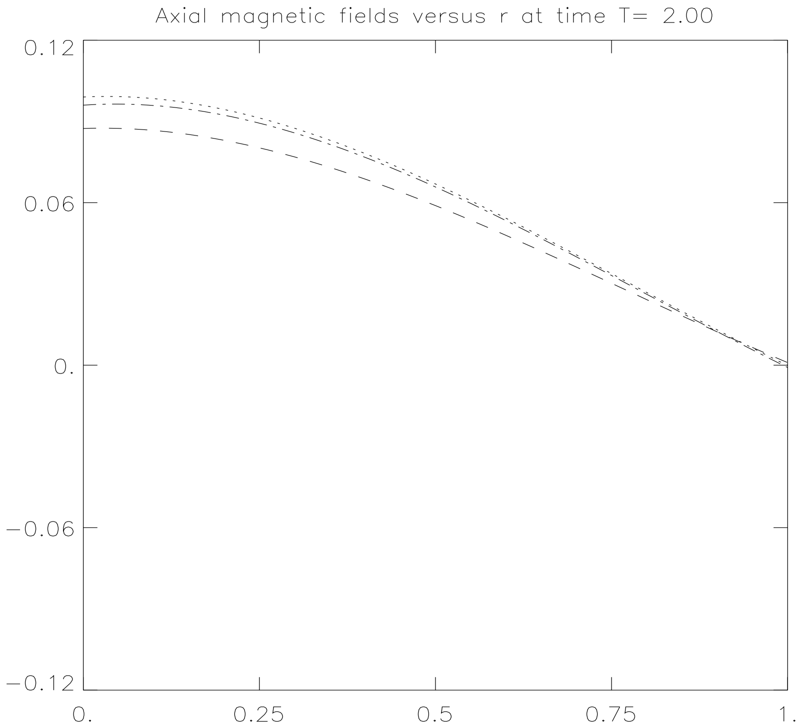

Fig. 7. Axial components after 1000 time-iterations of the velocities and magnetic fields: superposition of exact $(\cdots\cdots)$, first order $(- - - -)$ and second order $(- \cdot - \cdot - \cdot -)$ solutions.

5.2 Numerical diffusion coefficients

We estimate the diffusion effects of the scheme with the following method. If we suppose *a priori* that B evolves numerically with a diffusion equation

$$B_t - D\Delta B = 0, \tag{11}$$

then one can prove that B_r and B_θ are given by

$$\begin{cases} B_\theta(r,t) = B_\theta(r,0)\exp\left(-D_2\alpha^2 t/R_0^2\right), \\ B_z(r,t) = B_z(r,0)\exp\left(-D_3\beta^2 t/R_0^2\right), \end{cases}$$

thanks to the choice of Bessel profiles. The same formulas can be obtained for $u(r,t)$ in terms of the initial condition and with other diffusion coefficients. For example Fig. 8 shows the superposition of the corrected solution, $B_\theta(r,T)\exp\left(D_2\alpha^2 T/R_0^2\right)$, at time T and the initial condition $B_\theta(r,0)$. Hence hypothesis (11) is *a posteriori* justified. Moreover, we see on the results of Table 3 that each coefficient D follows approximately a linear law $D = \overline{D}h$.

meshes	8000	32000
h	$2\ 10^{-2}$	10^{-2}
Δt	$1.94\ 10^{-2}$	$6.7\ 10^{-4}$
$D_2(B_\theta)$	$1.3\ 10^{-3}$	$0.7\ 10^{-3}$
$D_2'(v_\theta)$	$3.5\ 10^{-3}$	$2\ 10^{-3}$
$D_3(B_z)$	$2\ 10^{-3}$	$1.2\ 10^{-3}$
$D_3'(v_z)$	$2\ 10^{-3}$	$1.2\ 10^{-3}$

Table 3: Numerical dissipation coefficients of the second order scheme

5.3 Sedov's strong-shock solution

We present the last validation test which is an extension to MHD of the hydrodynamical strong shock solution found by Sedov [22]. The extension is possible in the cylindrical case for a magnetic field orthogonal to the planar flow ($B = B_z e_z$) and for the adiabatic index of the gas $\gamma = 2$. Thus the total internal energy becomes $\rho\bar{\varepsilon} = p/(\gamma-1) + B_z^2/2 = p^*/(\gamma-1)$ where $p^* = p + B_z^2/2$ is the total pressure. The physical context of this case, detailed in [16,22], is the study of a shock wave generated by the ponctual release of a

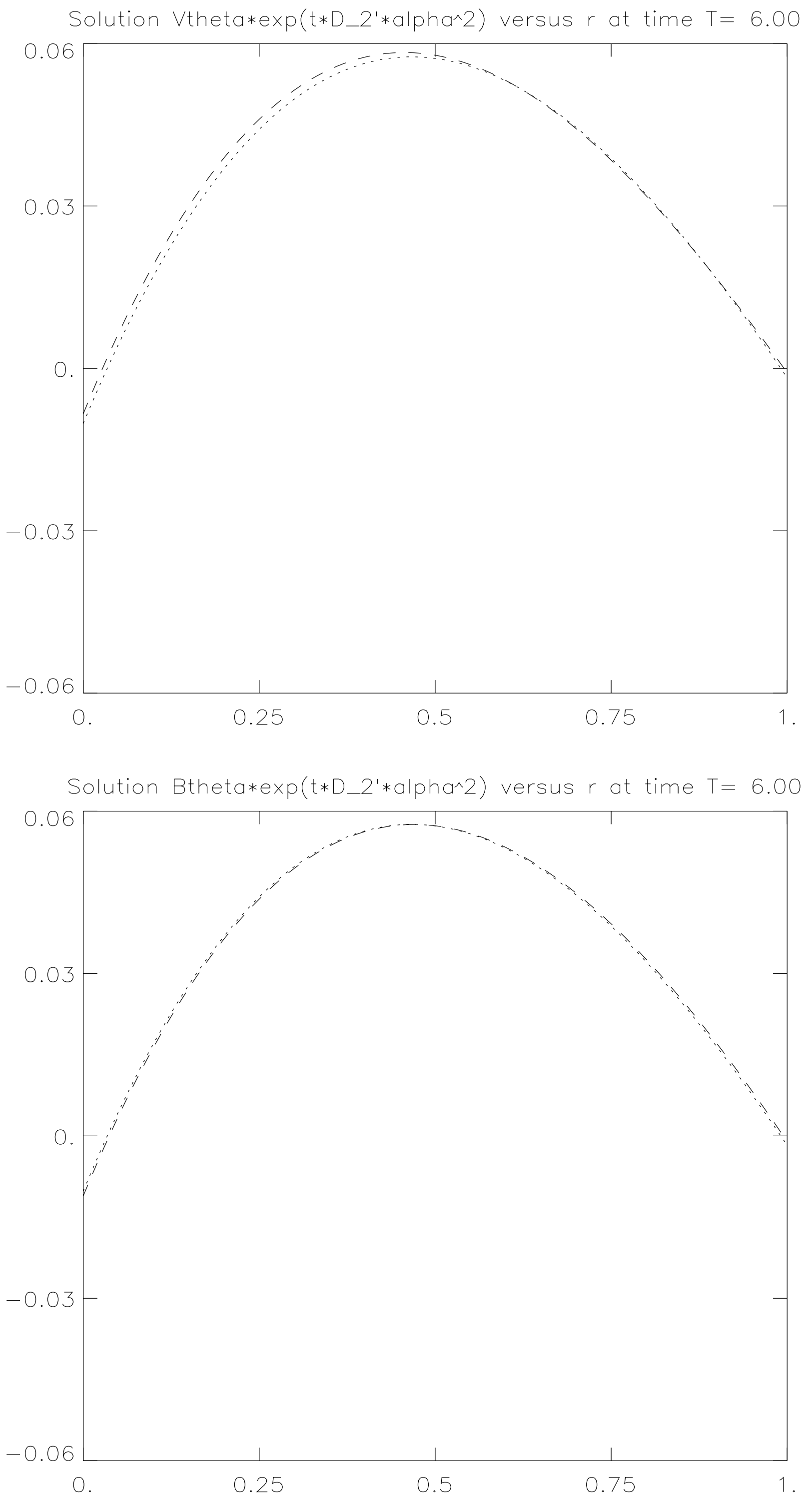

Fig. 8. Diffusion corrected solution ($- \cdot - \cdot -$), superposed to the exact solution (—), azimuthal components of the velocity and magnetic field (32000-cells mesh, second order scheme)

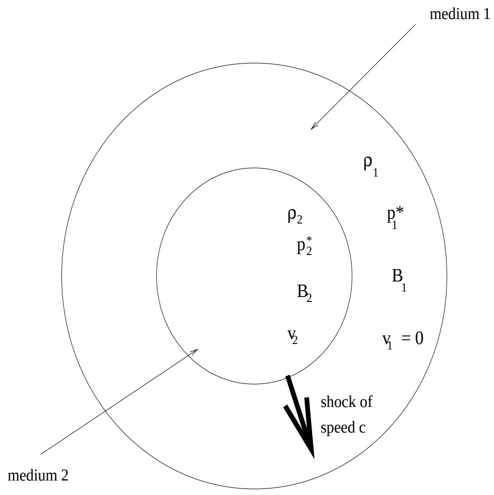

Fig. 9. Initial state for the stong-shock solution

large amount of energy in a gas at rest. Fig. 9 displays the initial state of the computation, which will be detailed hereafter.

The jump relations at the shock can be written as follows

$$\left\{\begin{aligned} \rho_2 &= \tfrac{\gamma+1}{\gamma-1}\rho_1\left(1+\tfrac{2}{\gamma-1}\tfrac{a_1^2}{c^2}\right)^{-1}, \\ u_2 &= \tfrac{2}{\gamma+1}c\left(1-\tfrac{a_1^2}{c^2}\right), \\ p_2^* &= \tfrac{2}{\gamma+1}\rho_1 c^2\left(1-\tfrac{\gamma-1}{2\gamma}\tfrac{a_1^2}{c^2}\right), \\ B_{z,2} &= \rho_2\tfrac{B_{z1}}{\rho_1}, \end{aligned}\right. \tag{12}$$

where $a_1^2 = \dfrac{\gamma\, p_1^*}{\rho_1}$ is the square of the sound speed in the external medium, c is the shock speed. In the strong shock approximation we suppose that the sound speed a_1 is very small with respect to the shock speed c. So the upstream pressure p_1^* has no influence on the downstream state and one seeks solutions depending only on one dimensionless parameter $\lambda = \left(\dfrac{\rho_1}{E_0}\right)^{\frac{1}{\nu+2}} \dfrac{r}{t^{\frac{2}{\nu+2}}}$ where the constant E_0 is proportional to the energy liberated per unit length and ν the dimension of the problem (here $\nu = 2$).

Thus one can find the shock speed and its position at any time

$$r^* = \lambda^* \left(\frac{\rho_1}{E_0}\right)^{\frac{1}{\nu+2}} t^{\frac{2}{\nu+2}}, c = \frac{dr^*}{dt} = \frac{2\lambda^*}{\nu+2}\left(\frac{\rho_1}{E_0}\right)^{\frac{1}{\nu+2}} t^{-\frac{\nu}{\nu+2}},$$

where λ^* is a constant taken equal to 1. Taking into account the strong shock hypothesis, one can find the simplified jump relations

$$\rho_2 = \frac{\gamma+1}{\gamma-1}\rho_1, u_2 = \frac{2}{\gamma+1}c, p_2^* = \frac{2}{\gamma+1}\rho_1 c^2, B_{z,2} = \rho_2\frac{B_{z1}}{\rho_1}.$$

On the other hand, if the position of the shock is r_0 at time t_0, then one can find its position and speed at any time

$$r^* = r_0\left(\frac{t}{t_0}\right)^{\frac{2}{\nu+2}}, c = \frac{2}{\nu+2}\frac{r_0}{t_0}\left(\frac{t}{t_0}\right)^{-\frac{\nu}{\nu+2}}.$$

Finally, we give the formulas for the internal rarefaction wave behind the shock after passing to the limit when γ tends to 2 (see Sedov [22] for the derivation)

$$\begin{cases} \dfrac{r}{r_2} &= \left[\frac{3}{4}(\nu+2)V\right]^{2\alpha_2}\left[3(1-\frac{\nu+2}{2}V)\right]^{2\alpha_2}\left[3((\nu+2)V-1)\right]^{-\alpha_2} \\ \dfrac{u}{u_2} &= \frac{(\nu+2)(\gamma+1)}{4}V\dfrac{r}{r_2}, \\ \dfrac{\rho}{\rho_2} &= \{3[(\nu+2)V-1]\}^{\alpha_3}\left[3(1-\frac{\nu+2}{2}V)\right]^{\frac{\nu-2}{\nu+2}}\exp\left[-4\alpha_3\frac{1-\frac{3}{4}(\nu+2)V}{1-\frac{\nu+2}{2}V}\right], \\ \dfrac{p}{p_2} &= \left[\frac{3}{4}(\nu+2)V\right]^{2\alpha_3}\left[3(1-\frac{\nu+2}{2}V)\right]^{\frac{2(\nu-2)}{\nu+2}}\exp\left[-4\alpha_3\frac{1-\frac{3}{4}(\nu+2)V}{1-\frac{\nu+2}{2}V}\right], \\ \dfrac{T}{T_2} &= \dfrac{p}{p_2}\dfrac{\rho_2}{\rho}, \end{cases} \quad (13)$$

where $\alpha_2 = \frac{-1}{2+\nu}, \alpha_3 = \frac{\nu}{2+\nu}$. V is such that $\frac{1}{\nu+2} \le V \le \frac{4}{3(\nu+2)}$ for $\nu = 1, 2$. Moreover r_2 is the position of the shock wave, ρ_2, u_2, p_2 and T_2 are respectively the density, velocity, pressure and temperature just behind the shock. In the numerical test we take $t_0 = 1$ as the initial time and the cylindrical shock is located at $r_0 = 0.5$. There is a strong jump on the total pressure from the upstream to the downstream states: $p_1^* \approx 10^{-6}$, $p_2^* \approx 10^{-2}$. Furthermore, near the center of the rarefaction wave (r going to 0), p tends to $p_0 = 3^{\frac{4(\nu-1)}{\nu+2}}4^{\frac{2-3\nu}{\nu+2}}\exp\left(\frac{-2\nu}{\nu+2}\right)p_2 \neq 0$ meanwhile ρ tends to 0. Hence the temperature tends to infinity . This solution is self-similar and one can compare the normalized solution at any time to the initial condition. For $t' = \sqrt{t/t_0}$ and $r' = r/t'$ we have the following relations

$$\rho(r,t) = \rho(r', t_0),\ u(r,t) = u(r', t_0)t',$$

$$p^*(r,t) = p^*(r', t_0)t,\ B_z(r,t) = B_z(r', t_0).$$

We plot on Fig. 10 the profiles of the density at the initial time and the normalized computed density at time $T = 3$ on the 32000-cells mesh with the second order scheme. The comparison between the two profiles shows that the shock propagates at the right speed and that the rarefaction wave is computed with a high precision.

6 Conclusion

In this paper, we present some numerical results obtained with the bidimensional second order version of the scheme introduced in [7]. This scheme is based on a flux-splitting formula, partly designed on kinetic ideas. An important property is that it is consistent with the $\nabla.B = 0$ condition. So there is no need to impose this constraint at each time-step. We believe that this property is very interesting with regard to the schemes based on Approximate Riemann Solvers. The scheme is robust as demonstrated by numerical tests and stable under a standard CFL condition. Moreover the scheme is simple thanks to flux splitting form and leads to a fast execution on super-scalar computers ($120\mu s$ per cell per time-step on a IBM RS 6000/550). One can improve the accuracy of the scheme by using other less diffusive limiters or by extending it to third order in space [1]. The axisymmetric version of the scheme is currently being developed in order to simulate higher dimension problems.

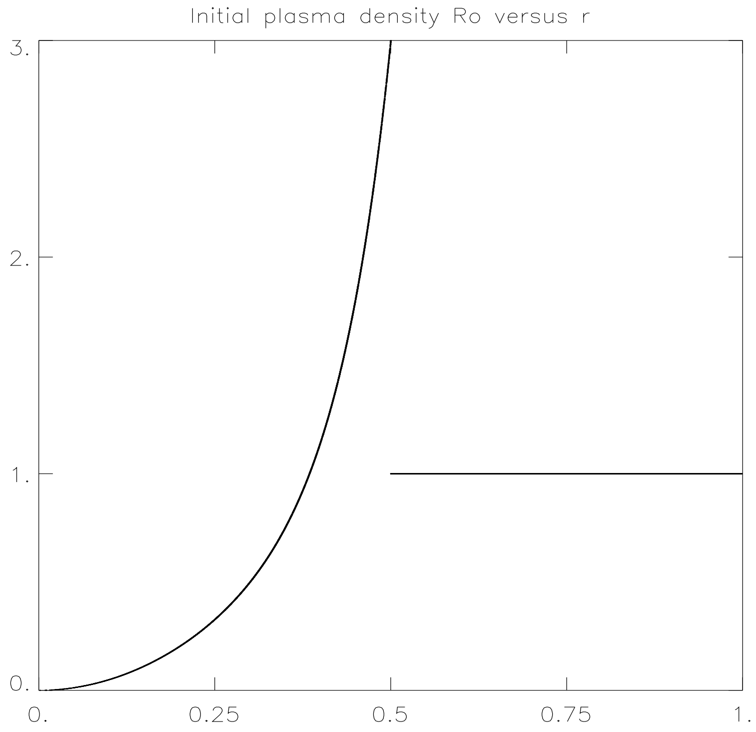

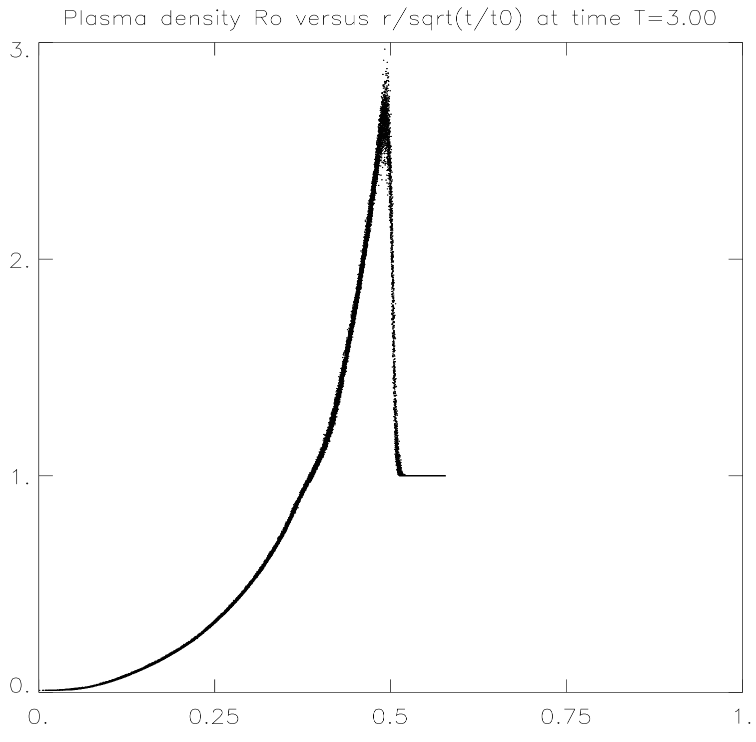

Fig. 10. Initial density and normalized density at time $T = 3$ computed with second order scheme on the 32000-cells mesh.

References

[1] R. Abgrall: Design of an essentially non-oscillatory reconstruction procedure on finite-element type meshes. Rapport INRIA No 1584, janvier 1992.

[2] T.J. Barth: Aspects of unstructured grids and finite-volume solvers for the Euler and Navier-Stokes equations. AGARD-FDP-VKI Report 787, Special course on unstructured grids methods for advection dominated flows, May 1992.

[3] F. Bouchut: personal communication.

[4] M. Brio, C.C. Wu: An upwind differencing scheme for the equations of ideal magnetohydrodynamics. J. Comp. Phys. 75 (1988) 400-422.

[5] S.Chandrasekhar: *Hydrodynamic and hydromagnetic stability*, Oxford University Press, 1961.

[6] P. Colella, A.L. Zachary: A higher-order Godunov method for the equations of ideal magnetohydrodynamics. J. Comp. Phys. 99 (1992) 341-347.

[7] J.P. Croisille, R. Khanfir, G. Chanteur: Numerical simulation of the MHD equations by a kinetic-type method. J. Scient. Comp. 10 (1995) 81-92.

[8] W. Dai, P.R. Woodward: An approximate Riemann solver for ideal magnetohydrodynamics. J. Comp. Phys. 111 (1994) 354-372.

[9] H. Deconninck, R. Struijs, G. Bourgois, H. Paillère, P.L. Roe: Multidimensional upwind methods for unstructured grids. AGARD-FDP-VKI Report 787, Special course on unstructured grids methods for advection dominated flows, May 1992.

[10] L.J. Durlofsky, S. Osher, B. Engquist: Triangle based TVD schemes for hyperbolic conservation laws. J. Comp. Phys. 98 (1992) 64-73.

[11] R. de Fainchtein, S.Z. Zalesak, R.L. Löhner, D.S. Spicer: Finite element simulation of a turbulent MHD system: comparison to a pseudo-spectral simulation. Comp. Phys. Comm. 86 (1995) 25-39.

[12] A. Harten, P.D. Lax, B. Van Leer: On upstream differencing and Godunov-type schemes for hyperbolic conservation laws. Siam review 25(1) (1983) 35-61.

[13] C. Hirsch: *Numerical computation of internal and external flows* vol. 1 and 2, A Wiley-Interscience publication, John Wiley & sons, 1988.

[14] R. Khanfir: Approximation volumes finis de type cinétique du système de la MHD idéale compressible à pression isotrope. Thèse de l'Université Paris 11 (1995).

[15] L. Landau, F. Lifchitz: *Electrodynamique des milieux continus*, Editions MIR Moscou (1969).

[16] L. Landau, F. Lifchitz: *Mécanique des fluides*, Editions MIR Moscou (1969).

[17] K. Lerbinger and J.F. Luciani, A New Semi-implicit Method for MHD Computations, J. Comp. Phys. 97 (1991) 444-459.

[18] B. Perthame: Boltzmann type schemes for gas dynamics and the entropy property, SIAM J. Num. Anal. 27(6) (1990) 1405-1421.

[19] B. Perthame: Second order Boltzmann schemes for compressible Euler equations in one and two space dimensions, SIAM J. Num. Anal. 29(1) (1992) 1-19.

[20] D.I. Pullin: Direct simulation methods for compressible inviscid ideal-gas flow, J. Comp. Phys. 34 (1980) 231-244.

[21] R.H. Sanders, K.H. Prendergast: The possible Relation of 3-Kiloparsec Arm to Explosion in the Galactic Nucleus. ApJ, 188 (1974).

[22] L. Sedov: *Similitudes et dimensions en mécanique*, Editions MIR, (1977).

[23] J.M. Stone, J.F. Hawley, C.R. Evans, M.L. Norman: A test suite for magnetohydrodynamical simulations. ApJ, 388 (1992), 415-437.

[24] J.M. Stone and M.L. Norman, ZEUS-2D: A radiation Magnetohydrodynamics Code for Astrophysical Flows in two Space Dimensions. II The Magnetohydrodynamic Algorithms and Tests, ApJ, 80 (1992), 791-818.

[25] Tanaka: Finite volume TVD schemes. Comp. Flu. Dyn. J. (1992) 1-14.

[26] P. Vankeirsbilck, H. Deconinck: Computation of inviscid supersonic flows using adaptative meshes. In Desideri and Periaux J, editors, Proceedings of the International workshop on hypersonic flows for reentry problems, Antibes, France (Jan. 1990) 22-25. Springer Verlag.

[27] B. Van Leer: Towards the ultimate conservative difference scheme V. A second order sequel to Godunov's method. J. Comp. Phys. 32 (1979) 101-136.

[28] S.Z. Zalesak, D.S. Spicer, R.L. Lohner, S.A. Curtis: The role of adaptative mesh refinement in MHD modelling of the magnetosphere. Proceedings of Spatio-Temporal Analysis for Resolving Plasma Turbulence (START), Aussois, France (1993) ESA WPP.